Supporting Information

©XMU and CCS

Ex Situ Rapid Evaluation of PEMFC Metallic Bipolar Plate Coatings under Dynamic Electrochemical Stress Conditions

Haoqing Zheng[a], Xia Sheng[b,*], Xiaodan Wen[a], Zhibo Liu[a], Yuxin Xie[a], Chunyu Ru[c], Dan Wang[c], Fangbing Liu[c], Ying Liu[c], Guangyu Chen[d,*], Shuaifeng Lou[a,*]

Dedication

a Haoqing Zheng ;Xiaodan Wen ; Zhibo Liu ; Yuxin Xie ; *Shuaifeng Lou
School of Chemistry and Chemical Engineering
Harbin Institute of Technology
Harbin, China
*Shuaifeng Lou (shuaifeng.lou@hit.edu.cn)

b *Xia Sheng
Powertrain Department
General R&D Institute of China FAW
Changchun, China
*Xia Sheng (shengxia@faw.com.cn)

c Chunyu Ru ; Dan Wang , Fangbing Liu ; Ying Liu
Commercial Vehicle Development Institute
FAWJiefang Automotive Co., Ltd.
Changchun, China

d *Guangyu Chen
Institute of Carbon Neutrality
Zhejiang Wanli University
Ningbo, China
E-mail:*Guangyu Chen (gychen@zwu.edu.cn)

ACCEPTED

Note S1. Basis and interpretation of the dynamic potential protocol

Note S2. Additional Multiscale SEM and EDS Characterization of the Corrosion Stages

Note S3. Comparison with a bipolar plate after 1000 h of actual stack operation

Note S4. Piecewise fitting and selection of approximate corrosion-stage boundaries

Note S1. Basis and interpretation of the dynamic potential protocol

The dynamic protocol contains two independently determined elements: the temporal structure and the electrochemical stress levels.

The temporal structure was adapted from the approximately 1800-s time framework of the CLTC-P driving cycle specified in GB/T 38146.1-2019. The repeated load-state concept was also informed by the fuel-cell durability cycles described in Annexes B and C of GB/Z 44116-2024. These standards were used to establish the approximate duration and sequence of different operating-state categories. Neither standard specifies the electrochemical potential of a metallic bipolar plate relative to an Ag/AgCl reference electrode.

The fuel-cell terminal voltage cannot be directly converted into the potential of a bipolar plate in a three-electrode cell. The terminal voltage represents the potential difference between the anode and cathode under load and contains contributions from activation, ohmic, and mass-transfer losses. In contrast, the value controlled in the present three-electrode experiment is the interfacial potential of the bipolar-plate working electrode relative to Ag/AgCl.

Moreover, the local bipolar-plate/electrolyte interfacial potential in an operating stack depends on the local gas composition, water content, pH, current distribution, electrical-contact condition, and reference scale. Its direct determination is therefore difficult. Previous in situ studies have also shown that the corrosion potential of a bipolar plate is not necessarily strongly coupled to the fuel-cell terminal voltage.

Accordingly, the potentials used in this study were not obtained by converting the terminal voltages associated with startup, idle, variable-load, or constant-speed operation. They were selected independently as controlled electrochemical stress levels for comparative ex situ corrosion testing.

The overall potential window was selected on the following basis. First, the U.S. Department of Energy metallic-bipolar-plate corrosion protocol uses 0.6 V vs Ag/AgCl under simulated cathode conditions at pH 3, 80 ℃, and in the presence of fluoride, providing a commonly used potentiostatic corrosion benchmark. Second, published dynamic corrosion studies on metallic bipolar plates have employed potentials extending approximately from 0.6 to 0.95 V under simulated PEMFC cathode conditions. Third, polarization studies of carbon-coated 316L stainless-steel bipolar plates have examined potential ranges extending approximately from -0.2 to 1.0 V vs Ag/AgCl. Finally, the preliminary experiments in the present study demonstrated a systematic increase in corrosion severity at 0.6, 0.8, and 1.0 V.

On this basis, 0.3 V was used as the lower boundary of the variable-potential segment; 0.7 and 0.8 V represented intermediate stress levels; 0.9 V represented a sustained high-potential stress; and 1.0 V represented a short severe high-potential stress. These assignments describe the relative electrochemical aggressiveness within the ex situ protocol. They do not imply that these values are the actual bipolar-plate potentials corresponding to specific vehicle operating stages.

After each dynamic-stress cycle, OCP was monitored for 1200 s, followed by a diagnostic Tafel polarization scan from -0.25 to +0.25 V relative to the OCP measured before the scan, at 1 $mV \cdot s^{-1}$ (1 mV per step, 1 s per step; approximately 500 s per scan). These conditions differ from the -0.5 to 1.4 V vs Ag/AgCl range and 2 $mV \cdot s^{-1}$ scan rate used for baseline LSV characterization. As illustrated by the representative trace in Fig. 5b, the OCP before the diagnostic scan was approximately -0.25 V vs Ag/AgCl, corresponding to a diagnostic scan range of approximately -0.50 to 0 V vs Ag/AgCl. This range lies below the 0.3-1.0 V vs Ag/AgCl window used for dynamic acceleration, suggesting a relatively small additional contribution to anodic corrosion from the diagnostic scans compared with the dynamic-stress steps. However, this contribution was not independently quantified, and scan-induced changes in the surface state cannot be excluded. Excluding diagnostic scan time from the cumulative dynamic-stress duration does not imply that the scans have no effect on degradation. Accordingly, the apparent acceleration factor should be interpreted as specific to the combined dynamic-stress and diagnostic-testing protocol used in this study.

ACCEPTED

Table S1. Definition and interpretation of the potential segments in the dynamic electrochemical stress protocol.

Potential segment	Applied potential (V vs Ag/AgCl)	Duration (s)	Physical interpretation
Short high-potential stress	1.0	2	Short-duration severe electrochemical stress
High-potential hold	0.9	396	Sustained high-potential electrochemical stress
Variable-potential segment	0.3–0.7	992	Cyclic low-to-intermediate electrochemical stress
Intermediate-potential hold I	0.8	198	Sustained intermediate-to-high electrochemical stress
Intermediate-potential hold II	0.7	198	Sustained intermediate electrochemical stress
Final short high-potential stress	1.0	2	Short-duration severe electrochemical stress

The durations were adapted from the temporal characteristics of the referenced duty cycles, whereas the applied potentials were independently selected from previously reported corrosion-test windows and the preliminary potential-screening results obtained in the present study. No direct conversion between vehicle operating voltage, fuel-cell terminal voltage, and bipolar-plate potential was performed. The individual potentials therefore represent relative electrochemical stress levels rather than the actual bipolar-plate potentials associated with specific vehicle operating stages.The six dynamic-stress steps listed in Table S1 have a total duration of 1788 s (29.8 min, approximately 0.5 h). The 2 s quiet period preceding the cyclic potential sweep, OCP monitoring, and diagnostic polarization measurement are excluded from this duration.

Table S2. Basis and interpretation of the temporal and potential parameters used in the dynamic electrochemical stress protocol.

Protocol parameter	Source	Role in the present protocol
Overall temporal framework	GB/T 38146.1-2019, Section 4.1 and Table 1	Provides the 1800-s CLTC-P framework
Operating-state proportions	GB/T 38146.1-2019, Table 1	Provides acceleration, deceleration, cruise, and idle proportions
Repeated load transitions	GB/Z 44116-2024, Sections 5.2.1.2 and 5.2.7.1, Annex B	Supports repeated steady-load and load-transition design
Stack durability cycle	GB/Z 44116-2024, Section 6.2.4(e) and Annex C	Supports the 1800-s dynamic current-cycle concept
Applied potentials	Published BPP corrosion studies and preliminary screening	Defines relative electrochemical stress levels

Table S3. Corrosion potential and corrosion current density obtained by Tafel fitting under different testing conditions. Data are presented as mean ± SD (n = 3)

Testing parameter	Condition	E_{corr} (mV vs. Ag/AgCl)	I_{corr} (10^{-8}A·cm^{-2})
Oxygen flow rate	20 mL·min^{-1}	49±7.54	2.69±0.11
	40 mL·min^{-1}	-0.74±9.03	3.81±0.19
Electrolyte pH	1	65.67±7.88	5.89±0.27
	2	52.67±5.91	4.68±0.19
	3	45.33±5.12	2.60±0.10
Temperature	60 ℃	-80.99±8.96	3.89±0.21
	70 ℃	-12.33±7.01	3.63±0.17
	80 ℃	45.67±7.40	2.71±0.15

Note S2. Additional Multiscale SEM and EDS Characterization of the Corrosion Stages

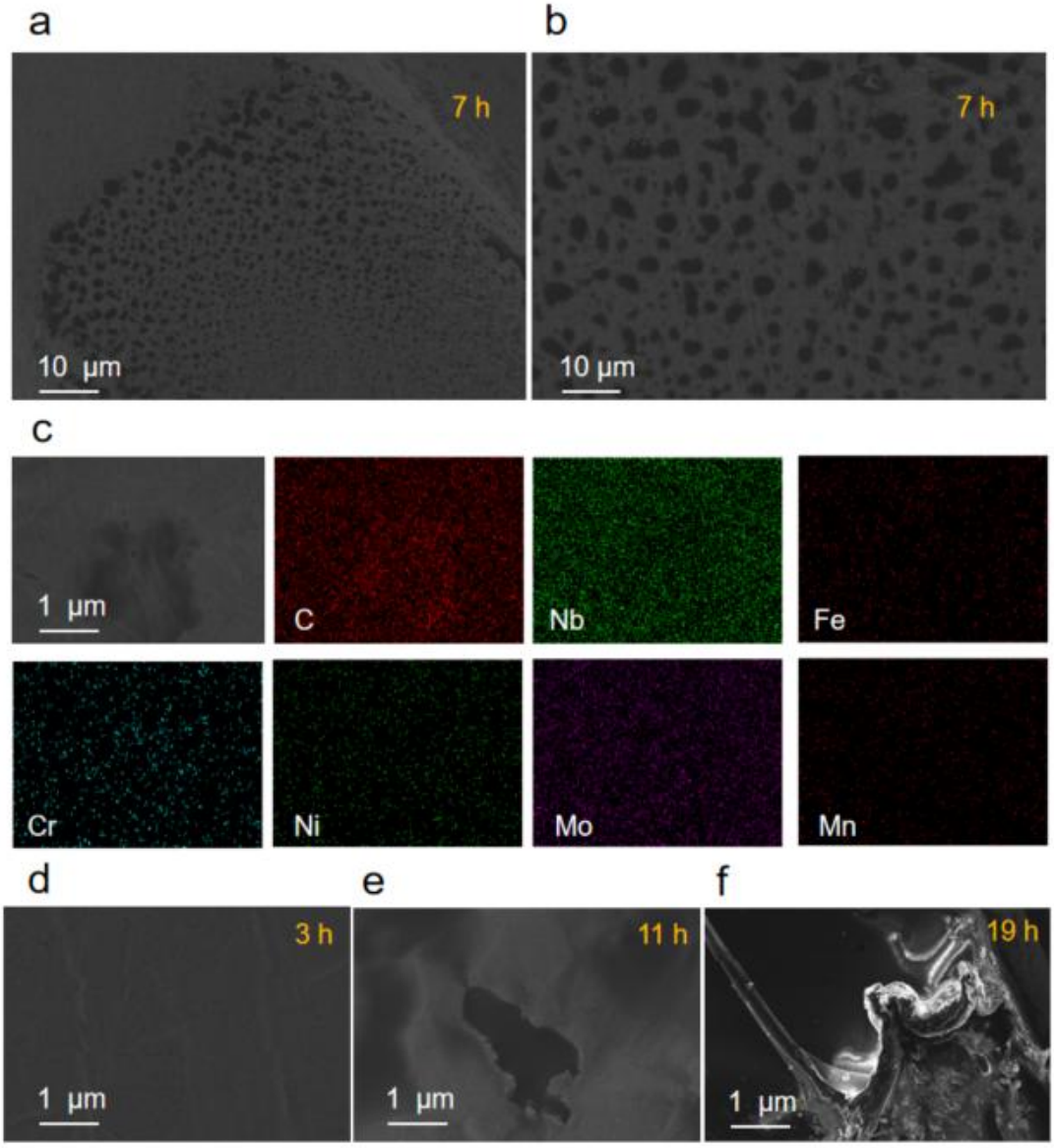

Fig. S1. Additional multiscale SEM and EDS characterization of the FBP at representative corrosion stages. All exposure times indicate cumulative dynamic-stress duration: (a, b) SEM images from different surface regions at 7 h, showing widespread honeycomb-like porous morphology associated with Stage II; (c) high-magnification SEM image of a representative damaged region at 7 h and the corresponding EDS elemental maps; (d) high-magnification SEM image at 3 h, showing subtle localized defects associated with Stage I; (e) high-magnification SEM image at 11 h, showing local coating penetration during the early period of Stage III; and (f) SEM image at 19 h, showing severe coating curling, rupture, and separation during the advanced period of Stage III.

Note S3. Comparison with a bipolar plate after 1000 h of actual stack operation

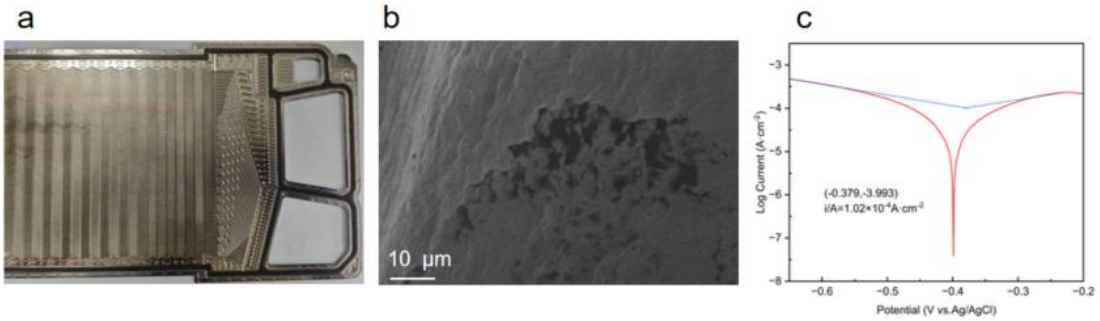

Fig. S2. Carbon-coated 316L stainless-steel bipolar plate retrieved after 1000 h of actual PEMFC stack operation: (a) optical photograph; (b) SEM image; and (c) Tafel polarization curve and fitting result.

A carbon-coated 316L stainless-steel bipolar plate was retrieved from a PEMFC stack after 1000 h of actual operation. The post-service plate was characterized by surface observation and Tafel polarization testing under the same electrochemical conditions used for the ex situ accelerated samples.As shown in Fig. S2, localized corrosion damage was observed on the surface of the stack-aged bipolar plate. Tafel fitting yielded a corrosion potential of approximately -0.379 V vs Ag/AgCl and a corrosion current density of 1.02×10^{-4} A·cm^{-2}. The corrosion current density was comparable to that measured for the ex situ accelerated sample after approximately 7 h.

Using the comparable corrosion-current-density state as the evaluation endpoint, the apparent acceleration factor was estimated from the cumulative dynamic-stress duration. The approximately 7 h specimen underwent 14 complete test cycles, corresponding to 6.953 h of cumulative dynamic-stress exposure. The quiet periods, OCP monitoring, and diagnostic polarization measurements were excluded from this duration.

Apparent acceleration factor = stack operating time / cumulative dynamic-stress duration ≈ 1000 h / 7 h ≈ 143.

This factor describes acceleration on a cumulative dynamic-stress-time basis, rather than on a total elapsed experimental-time basis.This comparison provides preliminary experimental support for the acceleration efficiency of the proposed ex situ protocol.

Note S4. Piecewise fitting and selection of approximate corrosion-stage boundaries

The 21 corrosion-current-density measurements at nominal cumulative dynamic-stress times of 0-20 h were analyzed using a continuous three-segment linear model equivalent to the PWL3 function in Origin. The untransformed corrosion current density, jcorr (A·cm^{-2}), was fitted against time, t (h), by unweighted least squares. Three segments were specified to examine the proposed three-stage description; the analysis did not independently establish the optimal number of segments.

The model was expressed as:
$j_{corr}(t) = a_1 + k_1 t + (k_2 - k_1)\max(0, t - t_1) + (k_3 - k_2)\max(0, t - t_2)$,
where t_1 and t_2 are the two breakpoints, a_1 is the intercept of the first segment, and k_1, k_2, and k_3 are the slopes of the three segments. The slope unit is A·cm^{-2}·h^{-1}. The model enforces continuity at both breakpoints.

An integer-grid search was conducted over all admissible breakpoint pairs. For counting observations, the three intervals were defined as $t < t_1$, $t1 \leqslant t < t_2$, and $t \geqslant t_2$, with at least three distinct data points assigned to each interval. Boundary observations were counted only once, and all 21 observations were included once in the fitting objective. These constraints yielded 91 admissible combinations. For each fixed breakpoint pair, the remaining model coefficients were estimated jointly by minimizing the total residual sum of squares (RSS). No sign constraints were imposed on the slopes or fitted current densities. All combinations were ranked by ascending RSS, as reported in Table S4.The n_1, n_2, and n_3

ACCEPTED

denote the numbers of observations assigned to the three intervals using the boundary convention specified in Note S4. R^2 refers to the overall fit. The fourth-ranked combination was selected for the morphology-informed stage description.

The three lowest-RSS combinations had breakpoints at 11 and 15 h, 11 and 14 h, and 11 and 16 h, respectively. All three placed the 3 and 7 h specimens within the same fitted interval and therefore did not distinguish the early pitting morphology observed at 3 h from the subsequent coating delamination observed at 7 h. Considering both the current-density trend and the SEM evidence, the fourth-ranked combination, with breakpoints at 3 and 9 h, was selected to describe the corrosion stages. Its RSS was 1.11115×10^{-8} $(A \cdot cm^{-2})^2$, compared with 1.04030×10^{-8} $(A \cdot cm^{-2})^2$ for the minimum-RSS combination.

For the selected breakpoints, the three nominal fitting intervals were 0-3, 3-9, and 9-20 h. Following the boundary-assignment convention above, these intervals contained 3, 6, and 12 observations, respectively. The fitted slopes were $k_1 = 4.66226 \times 10^{-6}$, $k_2 = 2.99023 \times 10^{-5}$, and $k3 = 1.40039 \times 10^{-6}$ $A \cdot cm^{-2} \cdot h^{-1}$, with $a_1 = -2.26913 \times 10^{-6}$ $A \cdot cm^{-2}$. The overall R^2 was 0.92207.

The selected boundaries are approximate, morphology-informed divisions rather than statistically optimal or precisely determined transition times. The SEM observations support differences between the sampled corrosion states but do not locate the transitions exactly at 3 and 9 h. The linear model is used to summarize trends rather than to describe corrosion kinetics mechanistically; in particular, its negative fitted value at 0 h has no physical interpretation and indicates a limitation in representing the early low-current region.

Table S4. Complete integer-grid search results for continuous three-segment linear fitting with at least three observations per segment, ranked by ascending residual sum of squares.

Rank	t_1 (h)	t_2 (h)	RSS ($(A/cm^2)^2$)	Overall R^2	k_1 ($A/cm^2/h$)	k_2 ($A/cm^2/h$)	k_3 ($A/cm^2/h$)	a_1 (A/cm^2)	n_1	n_2	n_3
1	11	15	1.040299E-08	0.927038	2.280708E-05	-1.342702E-05	1.323680E-05	-3.080404E-05	11	4	6
2	11	14	1.066994E-08	0.925165	2.302796E-05	-1.811579E-05	9.977952E-06	-3.154030E-05	11	3	7
3	11	16	1.087480E-08	0.923728	2.243457E-05	-9.588203E-06	1.667171E-05	-2.956233E-05	11	5	5
4	3	9	1.111146E-08	0.922069	4.662256E-06	2.990232E-05	1.400392E-06	-2.269133E-06	3	6	12
5	4	9	1.152854E-08	0.919143	1.126442E-05	3.121366E-05	1.285042E-06	-9.110067E-06	4	5	12
6	11	17	1.178011E-08	0.917379	2.200633E-05	-6.490280E-06	2.082227E-05	-2.813487E-05	11	6	4
7	5	9	1.224494E-08	0.914119	1.590261E-05	3.211868E-05	1.316857E-06	-1.621583E-05	5	4	12
8	10	16	1.230541E-08	0.913695	2.358917E-05	-4.339628E-06	1.409836E-05	-3.285704E-05	10	6	5
9	10	15	1.236653E-08	0.913266	2.378944E-05	-5.910935E-06	1.091421E-05	-3.345784E-05	10	5	6
10	9	16	1.247690E-08	0.912492	2.526751E-05	-1.084828E-06	1.235451E-05	-3.758531E-05	9	7	5
11	3	8	1.248119E-08	0.912462	2.845527E-06	3.390256E-05	2.940449E-06	-1.057980E-06	3	5	13
12	9	17	1.259045E-08	0.911696	2.503989E-05	-1.948615E-07	1.575281E-05	-3.697833E-05	9	8	4
13	10	17	1.266496E-08	0.911173	2.327852E-05	-2.714119E-06	1.787874E-05	-3.192508E-05	10	7	4
14	9	15	1.268808E-08	0.911011	2.535369E-05	-1.706707E-06	9.483492E-06	-3.781514E-05	9	6	6
15	4	8	1.275676E-08	0.910529	9.956810E-06	3.661622E-05	2.760655E-06	-7.802459E-06	4	4	13
16	10	14	1.296175E-08	0.909091	2.377363E-05	-6.975797E-06	7.900374E-06	-3.341040E-05	10	4	7
17	6	9	1.309455E-08	0.908160	1.947971E-05	3.214184E-05	1.544455E-06	-2.327670E-05	6	3	12
18	9	18	1.316088E-08	0.907695	2.466558E-05	9.505257E-07	1.862714E-05	-3.598017E-05	9	9	3
19	9	14	1.321142E-08	0.907340	2.520006E-05	-1.652034E-06	6.812928E-06	-3.740546E-05	9	5	7
20	11	18	1.322339E-08	0.907256	2.150728E-05	-3.696607E-06	2.482653E-05	-2.647138E-05	11	7	3
21	3	10	1.331158E-08	0.906638	8.364767E-06	2.560496E-05	4.624315E-07	-4.737473E-06	3	7	11
22	12	15	1.333964E-08	0.906441	2.092093E-05	-2.070520E-05	1.352703E-05	-2.363400E-05	12	3	6
23	10	13	1.339840E-08	0.906029	2.375031E-05	-8.720341E-06	5.940174E-06	-3.334046E-05	10	3	8
24	5	8	1.352466E-08	0.905143	1.515300E-05	3.940650E-05	2.727236E-06	-1.521635E-05	5	3	13
25	10	18	1.355338E-08	0.904942	2.285314E-05	-9.705950E-07	2.129537E-05	-3.064895E-05	10	8	3
26	9	13	1.356061E-08	0.904891	2.501959E-05	-1.558375E-06	5.136779E-06	-3.692420E-05	9	4	8
27	4	7	1.382378E-08	0.903046	8.426442E-06	4.565423E-05	4.019135E-06	-6.272092E-06	4	3	14
28	4	10	1.383541E-08	0.902964	1.419944E-05	2.576082E-05	5.015630E-07	-1.204509E-05	4	6	11
29	3	7	1.385749E-08	0.902809	8.614860E-07	3.981330E-05	4.274023E-06	2.647140E-07	3	4	14
30	9	12	1.391697E-08	0.902392	2.453981E-05	3.378943E-10	3.522828E-06	-3.564479E-05	9	3	9
31	12	16	1.404022E-08	0.901527	2.052217E-05	-1.399081E-05	1.705369E-05	-2.217188E-05	12	4	5
32	3	11	1.440718E-08	0.898954	1.104919E-05	2.276891E-05	-8.834032E-07	-6.527087E-06	3	8	10
33	5	10	1.440848E-08	0.898945	1.824005E-05	2.517758E-05	7.246885E-07	-1.933242E-05	5	5	11
34	8	11	1.469715E-08	0.896920	2.286870E-05	1.487220E-05	9.687640E-07	-3.052481E-05	8	3	10
35	6	10	1.479047E-08	0.896266	2.125775E-05	2.333309E-05	1.169972E-06	-2.624010E-05	6	4	11
36	7	10	1.482397E-08	0.896031	2.196425E-05	2.261293E-05	1.324206E-06	-2.802945E-05	7	3	11
37	4	11	1.484202E-08	0.895904	1.618365E-05	2.243402E-05	-7.210382E-07	-1.402930E-05	4	7	10
38	7	11	1.495214E-08	0.895132	2.252470E-05	1.782266E-05	5.311105E-07	-2.915036E-05	7	4	10
39	6	11	1.508663E-08	0.894188	2.212585E-05	1.933290E-05	2.280347E-07	-2.768694E-05	6	5	10
40	5	11	1.514140E-08	0.893804	1.965352E-05	2.139754E-05	-3.566692E-07	-2.121704E-05	5	6	10
41	12	17	1.515808E-08	0.893687	2.008409E-05	-9.262830E-06	2.119242E-05	-2.056558E-05	12	5	4
42	3	6	1.524274E-08	0.893093	-1.348168E-06	4.956953E-05	5.457508E-06	1.737816E-06	3	3	15
43	8	17	1.571834E-08	0.889758	2.606131E-05	2.721088E-06	1.224526E-05	-3.797425E-05	8	9	4
44	8	16	1.579648E-08	0.889210	2.612515E-05	2.484953E-06	9.511451E-06	-3.812320E-05	8	8	5
45	8	12	1.585418E-08	0.888805	2.422399E-05	8.171168E-06	2.186081E-06	-3.368715E-05	8	4	9
46	8	18	1.593571E-08	0.888233	2.580436E-05	3.314513E-06	1.404279E-05	-3.737469E-05	8	10	3
47	8	15	1.601989E-08	0.887643	2.599836E-05	2.665126E-06	7.114166E-06	-3.782734E-05	8	7	6
48	8	13	1.622869E-08	0.886178	2.507643E-05	5.074496E-06	3.478955E-06	-3.567617E-05	8	5	8
49	8	14	1.624273E-08	0.886080	2.557857E-05	3.641061E-06	4.853199E-06	-3.684784E-05	8	6	7
50	12	18	1.676773E-08	0.882398	1.959458E-05	-5.400448E-06	2.498907E-05	-1.877070E-05	12	6	3
51	7	12	1.687689E-08	0.881632	2.414308E-05	1.220349E-05	1.331525E-06	-3.238712E-05	7	5	9
52	13	16	1.754922E-08	0.876917	1.881992E-05	-2.035362E-05	1.691335E-05	-1.504618E-05	13	3	5
53	6	12	1.757851E-08	0.876711	2.405328E-05	1.464880E-05	6.818867E-07	-3.089933E-05	6	6	9
54	7	13	1.795856E-08	0.874046	2.530721E-05	8.979308E-06	2.278311E-06	-3.471537E-05	7	6	8

55	7	14	1.848060E-08	0.870384	2.610121E-05	7.122928E-06	3.321232E-06	-3.630338E-05	7	7	7
56	5	12	1.849088E-08	0.870312	2.213984E-05	1.716567E-05	-2.028608E-07	-2.453214E-05	5	7	9
57	7	17	1.860604E-08	0.869505	2.723153E-05	5.016447E-06	9.153069E-06	-3.856401E-05	7	10	4
58	7	18	1.865162E-08	0.869185	2.709836E-05	5.248921E-06	9.888629E-06	-3.829766E-05	7	11	3
59	7	16	1.867747E-08	0.869004	2.712503E-05	5.169102E-06	7.081959E-06	-3.835102E-05	7	9	5
60	3	12	1.868093E-08	0.868979	1.518002E-05	1.953306E-05	-1.214012E-06	-9.280978E-06	3	9	9
61	7	15	1.871019E-08	0.868774	2.678273E-05	5.768185E-06	5.166133E-06	-3.766641E-05	7	8	6
62	4	12	1.879066E-08	0.868210	1.935941E-05	1.870629E-05	-8.304160E-07	-1.720506E-05	4	8	9
63	13	17	1.882382E-08	0.867977	1.838546E-05	-1.273587E-05	2.092251E-05	-1.330832E-05	13	4	4
64	6	13	1.929131E-08	0.864698	2.555552E-05	1.160405E-05	1.308812E-06	-3.340305E-05	6	7	8
65	6	14	2.035070E-08	0.857268	2.666739E-05	9.639402E-06	2.029440E-06	-3.525617E-05	6	8	7
66	13	18	2.051257E-08	0.856133	1.791580E-05	-7.254366E-06	2.424365E-05	-1.142971E-05	13	5	3
67	5	13	2.106767E-08	0.852240	2.417385E-05	1.418795E-05	1.147545E-07	-2.724415E-05	5	8	8
68	6	15	2.109305E-08	0.852062	2.764404E-05	8.131912E-06	3.472670E-06	-3.688393E-05	6	9	6
69	6	16	2.136270E-08	0.850171	2.823077E-05	7.302602E-06	4.914382E-06	-3.786181E-05	6	10	5
70	6	18	2.142369E-08	0.849743	2.854252E-05	6.892335E-06	6.016956E-06	-3.838138E-05	6	12	3
71	6	17	2.142380E-08	0.849742	2.853282E-05	6.906659E-06	6.331454E-06	-3.836522E-05	6	11	4
72	4	13	2.206418E-08	0.845251	2.205113E-05	1.592816E-05	-7.917454E-07	-1.989678E-05	4	9	8
73	14	17	2.225038E-08	0.843945	1.694746E-05	-1.802106E-05	2.020113E-05	-6.758851E-06	14	3	4
74	3	13	2.243100E-08	0.842678	1.878050E-05	1.701169E-05	-1.414909E-06	-1.168129E-05	3	10	8
75	5	14	2.287843E-08	0.839540	2.576266E-05	1.211660E-05	4.978848E-07	-2.936256E-05	5	9	7
76	14	18	2.398483E-08	0.831780	1.649819E-05	-9.637592E-06	2.279866E-05	-4.812016E-06	14	4	3
77	5	15	2.433924E-08	0.829294	2.717670E-05	1.047331E-05	1.508741E-06	-3.124794E-05	5	10	6
78	4	14	2.454706E-08	0.827837	2.423342E-05	1.389106E-05	-7.171248E-07	-2.207907E-05	4	10	7
79	5	16	2.509523E-08	0.823992	2.812457E-05	9.449419E-06	2.412445E-06	-3.251177E-05	5	11	5
80	3	14	2.543362E-08	0.821619	2.178247E-05	1.508730E-05	-1.607884E-06	-1.368261E-05	3	11	7
81	5	17	2.544579E-08	0.821533	2.871890E-05	8.845012E-06	3.063384E-06	-3.330422E-05	5	12	4
82	5	18	2.552071E-08	0.821008	2.894846E-05	8.615585E-06	1.485238E-06	-3.361029E-05	5	13	3
83	4	15	2.668769E-08	0.812823	2.620235E-05	1.222772E-05	-9.972945E-08	-2.404800E-05	4	11	6
84	15	18	2.776851E-08	0.805243	1.516909E-05	-1.173219E-05	1.886989E-05	1.820390E-06	15	3	3
85	4	16	2.795834E-08	0.803911	2.760774E-05	1.111463E-05	3.129671E-07	-2.545339E-05	4	12	5
86	3	15	2.813833E-08	0.802649	2.452720E-05	1.347614E-05	-1.331512E-06	-1.551243E-05	3	12	6
87	4	17	2.866577E-08	0.798950	2.857252E-05	1.039107E-05	2.668130E-07	-2.641816E-05	4	13	4
88	4	18	2.891168E-08	0.797225	2.907829E-05	1.002260E-05	-2.457354E-06	-2.692394E-05	4	14	3
89	3	16	2.987510E-08	0.790468	2.656812E-05	1.234555E-05	-1.343820E-06	-1.687304E-05	3	13	5
90	3	17	3.093780E-08	0.783015	2.804455E-05	1.156755E-05	-1.990146E-06	-1.785733E-05	3	14	4

Author Contributions

Haoqing Zheng: Investigation, Methodology, Formal analysis, Writing – Original Draft.**Xia Sheng**: Supervision, Project administration, Writing – Review & Editing.**Xiaodan Wen**: Investigation, Data Curation.**Zhibo Liu**: Methodology, Validation.**Yuxin Xie**: Formal analysis, Visualization.**Chunyu Ru**: Investigation, Validation.**Dan Wang**: Data Curation, Visualization.**Fangbing Liu**: Resources, Investigation.**Ying Liu**: Validation, Formal analysis.**Guangyu Chen**: Writing – Review & Editing, Resources.**Shuaifeng Lou**: Conceptualization, Supervision, Project administration, Writing – Review & Editing. All authors reviewed the manuscript.

ACCEPTED